Materials Science & Engineering A 798 (2020) 140274

Contents lists available at ScienceDirect

Materials Science & Engineering A

journal homepage: http://www.elsevier.com/locate/msea

Strain rate and mechanical stability in determining deformation behavior of beta Ti alloys

S. Sadeghpour [a,*], V. Javaheri [a], S. Bruschi [b], J. Kömi [a], P. Karjalainen [a]

[a] Centre for Advanced Steels Research, University of Oulu, 90014, Oulu, Finland
[b] Industrial Engineering Department, University of Padua, 35131, Padova, Italy

ARTICLE INFO

Keywords:
Beta Ti alloys
Deformation mechanisms
Strain rate sensitivity
Deformation-induced martensite
Twinning
Dislocation slip

ABSTRACT

The effect of strain rate on flow behaviors of three beta Ti alloys with different beta phase stability was studied. The alloys were subjected to compression deformation at four strain rates ranging from 7×10^{-5} to 7×10^{-2} s^{-1} at room temperature. Microstructure evolution was characterized using laser scanning microscopy and electron backscattered diffraction methods. The effect of strain rate on the yield strength was found to vary between the alloys increasing with increased stability. The microstructural observations showed that the alloys exhibited different deformation mechanisms: deformation induced martensite formation, twinning and slip band formation. The strain hardening exponent (n) depended on the deformation mechanism, i.e., the stability. In the low and intermediate stability alloys showing martensite formation and combination of the deformation mechanisms respectively, n was about 0.07 independent of strain rate. In the alloy with the highest stability it was only 0.01 when the deformation mechanism was dislocation slip at low strain rates but increased significantly to ≈0.13 at high strain rates when also twinning occurred. The strain rate sensitivity factor (m) was about 0.014 and 0.017 for the low and intermediate stability alloy respectively independent of strain, but very low ≈ 0.002 for the highest stability alloy though increasing to ≈ 0.011 with increasing strain. Based on the experiments, the stability-strain rate-mechanism diagram was introduced to predict the effect of phase stability and strain rate on the deformation mechanism of beta Ti alloys.

1. Introduction

As an important alloy system, body centered cubic (BCC) crystal structured beta Ti alloys are being used in different industries such as aerospace, chemicals and biomedical thanks to their high specific strength, excellent corrosion resistance and biocompatibility [1,2]. These alloys possess a wide range of mechanical properties due to different deformation mechanisms including deformation-induced martensite (DIM) formation, twinning and dislocation slip. Various factors such as chemical composition, temperature, stress state and strain rate may affect deformation mechanisms.

Depending on the beta phase stability, different deformation mechanisms can be activated as controlling mechanism during deformation [3]. With increasing the beta phase stability, deformation mechanism changes from DIM to twinning and then to dislocation slip [4,5]. When the stability is low, beta Ti alloys typically exhibit a low yield strength (YS) but a high elongation [6,7]. In contrast, the alloys with high beta phase stability, generally display a high YS thanks to the solid solution effect, but a very low ductility [6,7].

Strain rate is one of the important processing parameters affecting deformation behavior of beta Ti alloys. Generally, the YS of metals and alloys with BCC crystal structure shows a positive strain rate sensitivity (SRS) because the thermal activation energy required to overcome on Peierls stress increases with increasing strain rate [8]. In contrast, strain hardening rate usually decreases with increasing strain rate as thermal softening caused by adiabatic heating opposes strain hardening effect. Several efforts have been devoted to evaluate the effect of strain rate on mechanical properties of beta Ti alloys including the stabilized beta Ti alloys which show dislocation slip as a sole deformation mechanism [9–11], the alloys with low stability exhibiting DIM formation [12–14] and the alloys with moderate stability which are susceptible to twinning [8,15,16]. However, a comparative study on the effect of strain rate on mechanical properties of beta Ti alloys with different levels of mechanical stability has rarely been done. Given that different mechanical stabilities lead to different deformation mechanisms, the effect of strain rate on plastic behavior could also be different. In addition, the strain

* Corresponding author.
E-mail address: saeed.sadeghpour@oulu.fi (S. Sadeghpour).

https://doi.org/10.1016/j.msea.2020.140274
Received 29 July 2020; Received in revised form 10 September 2020; Accepted 12 September 2020
Available online 12 September 2020

rate dependence of the YS can vary due to the chemical composition of the alloy. For instance, Li et al. [13] found for the Ti–10V–1Fe–3Al (wt. %) alloy, exposing the DIM transformation, that YS increased with increasing strain rate showing a linear relationship with logarithm of strain rate. In another work by Zhan et al. [8], it was found that in a beta Ti–25Nb–3Zr–3Mo–2Sn alloy, exhibiting a combination of transformation-induced plasticity (TRIP) and twinning-induced plasticity (TWIP) effects, YS and strain hardening rate were almost independent of strain rate. Ji et al. [15] demonstrated that in a beta Ti–10Mo–1Fe alloy, exhibiting the TWIP effect, YS increased but the strain hardening rate, tensile strength and elongation decreased with increasing strain rate.

In addition, in certain alloys, the deformation mechanism can be different at low and high strain rates. Ahmed et al. [16] reported a change in deformation mechanism from DIM formation to twinning with increasing the strain rate during deformation of a TRIP/TWIP beta Ti alloy. Kapoor et al. [17] also showed for a Zr alloy that the dominant deformation mechanism changed from dislocation slip to mechanical twinning with increasing the strain rate. This means that SRS on one hand may depend on the type of deformation mechanism and on the other hand strain rate may change the deformation mechanism. In fact, there is a synergy between SRS and deformation mechanism.

Though that different deformation mechanisms can be observed in beta Ti alloys which may result in different strain rate dependency, the effect of strain rate on microstructural evolution and mechanical properties of these alloys has not been clarified systematically. Therefore, the present study investigates the SRS of YS and the effect of strain rate on deformation mechanisms in three beta titanium alloys possessing different levels of beta phase stability.

2. Materials and methods

Three alloys in the alloying system of Ti–Al–Mo–V–Cr coded Ti-4733, Ti-3573 and Ti-3873 have recently been designed by using the d–electron method so that they exhibit different deformation mechanisms. Details of the designing procedure has been reported in the previous papers [3,18]. The chemical compositions of the alloys, which were melted twice using vacuum arc process, are listed in Table 1.

After homogenizing at 1100 °C for 4 h, the alloys were subjected to hot rolling at same temperatures. Then, secondary hot rolling was performed at 750 °C to the final thickness of 20 mm. Finally, the strips were solution annealed at 1000 °C for 0.5 h and subsequently quenched in water. To investigate the effect of strain rate, cylindrical samples with the dimensions of 8 mm in diameter and 12 mm in height were cut using electrical discharge machining perpendicular to the rolling direction. Interrupted compression tests were performed using an Instron 8502 machine at room temperature at different strain rates of 7×10^{-5}, 7×10^{-4}, 7×10^{-3} and 7×10^{-2} s^{-1} up to a constant engineering strain of 10%, at which the microstructure of deformed samples was investigated. Molybdenum disulfide was used as lubricant to reduce the friction between the sample and anvils during the compression tests.

To examine the microstructures, the deformed specimens were sectioned along their compression axis. Specimens were etched in a modified Kroll's reagent (6% HF + 18% HNO_3 + 76% H_2O) after standard metallographic preparation techniques. Microstructures were examined with a laser scanning confocal microscope (VK-X200, Keyence Ltd.). Moreover, electron backscatter diffraction (EBSD) scans were performed using a field emission gun Zeiss Sigma scanning electron microscope operating at 15 kV with a step size ranging from 0.5 to 0.05 μm. Samples for EBSD scans were first mechanically polished down to 1 μm and then chemically polished with a 1:5 solution of H_2O_2 and OP-S (oxide polishing suspension from Struers, a colloidal silica suspension with a pH of 9.8 and a grain size of 0.04 μm). Phase identification was performed using a Rigaku SmartLab 9 kW X-ray diffraction (XRD) system with Co-Kα radiation (λ = 0.179 nm) in the angular (2θ) range of 40–130°. The scan rate and step size were 7°/min and 0.05°, respectively.

Table 1
Chemical composition of the studied alloys (wt.%).

Alloy	Al	Mo	V	Cr	Ti
Ti-4733	4.2	7.1	3.1	2.9	Balance
Ti-3573	2.9	4.8	7.1	2.8	Balance
Ti-3873	2.9	7.9	7.0	3.0	Balance

3. Results

3.1. Stability of the alloys

The stability of beta phase in Ti alloys is usually presented by the Mo equivalent (Mo_{eq}) [19] and two alloying parameters of $\overline{Md}$ and $\overline{Bo}$, which are the average values of d-orbital energy level and the bond order respectively [20]. The higher the Mo_{eq} value, the higher the beta phase stability. The lower $\overline{Md}$ and the higher $\overline{Bo}$ are associated with the higher stability of the beta phase. According to the calculated values of these parameters listed in Table 2, the mechanical stability of beta phase in the present alloys is expected to vary in the order of Ti-4733<Ti-3573<Ti-3873.

The electronic parameters of $\overline{Md}$ and $\overline{Bo}$ have been shown to be very useful for predicting the deformation mechanisms occurring in an alloy which is actually done using the $\overline{Bo}$-$\overline{Md}$ map [21]. Fig. 1a shows the position of the present alloys on the $\overline{Bo}$-$\overline{Md}$ diagram and accordingly the alloys are called as low stability, intermediate stability and high stability alloy. As seen, the low stability alloy Ti-4733 belongs to the martensitic transformation region while the intermediate stability alloy Ti-3573 locates on the boundary of martensite formation/twinning, i.e. TRIP/TWIP, regions. The location of Ti-3873, the high stability alloy, is close to the boundary of TWIP/slip regions. The d–electron predictions have been confirmed by the previous experimental investigations [3], where the deformation mechanisms were found to be DIM formation, DIM/twinning and dislocation slip for Ti-4733, Ti-3573 and Ti-3873, respectively. However, the present study is focused on the effect of strain rate on these deformation mechanisms and microstructural evolution during compressive deformation. Fig. 1 also shows the initial microstructures and the corresponding XRD patterns of the solution treated alloys. As seen, all the alloys consist of single beta phase with the average grain size in the range of 150–200 μm.

3.2. Flow stress curves of the alloys

The true stress–true strain curves of the alloys compressed up to the engineering strain of 10% are presented in Fig. 2. It is seen that with increasing the phase stability (i.e. increasing the Mo_{eq}) the strength of alloys increases in the order of Ti-4733<Ti-3573<Ti-3873.

It is also noticed that the flow stress of the alloys is affected by the strain rate so that the sensitivity of their flow stress to the strain rate is Ti-4733>Ti-3573>Ti-3873 in the inverse order of their stability. Two variables, YS and strain hardening exponent (n) were used to evaluate the effect of strain rate. Given that the yield point of some beta Ti alloys is not well defined based on the shape of the stress-strain curve (especially compression curve), an offset yield point is usually defined. Thus, the YS of the present alloys was measured using the 0.2% offset method.

Table 2
Stability parameters of the studied alloys.

Alloy	Mo_{eq}	$\overline{Md}$	$\overline{Bo}$
Ti-4733	9.617	2.369	2.774
Ti-3573	11.137	2.356	2.778
Ti-3873	14.490	2.348	2.782

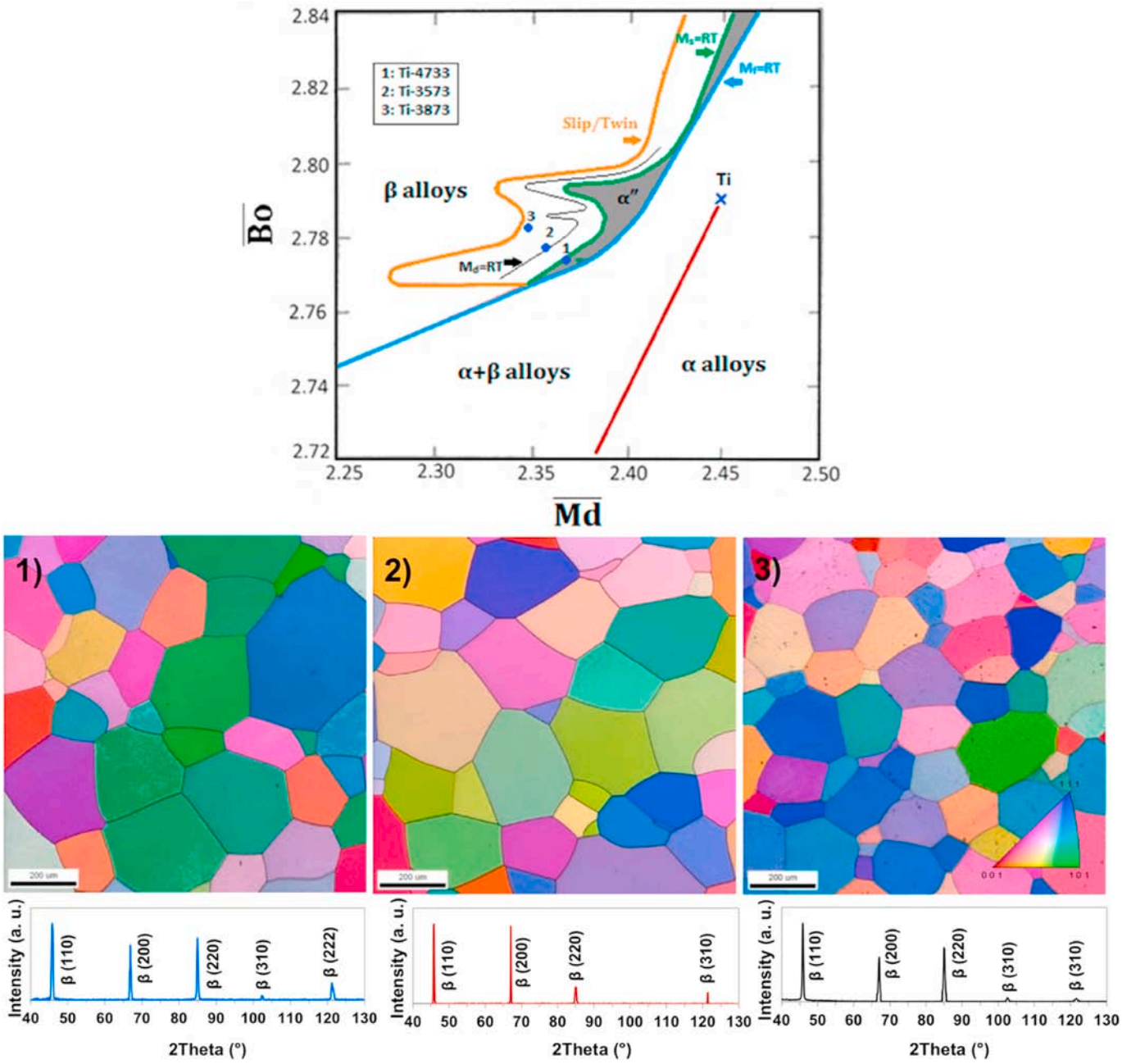

Fig. 1. The present alloys on the $\overline{Bo}$-$\overline{Md}$ stability diagram along with their initial microstructures and corresponding XRD patterns after annealing at 1000 °C for 0.5 h. The numbers of 1, 2 and 3 are related to Ti-4733, Ti-3573 and Ti-3873 as described in the legend box.

The strain hardening exponent representing the balance of work hardening and softening, was calculated according to Hollomon equation, $\sigma = K\varepsilon^n$, as follows [22]:

$$n = \frac{d(\ln \sigma)}{d(\ln \varepsilon)} \tag{1}$$

where σ and ε are the true stress and true strain. The variation of YS and n with strain rate are presented in Fig. 3a and b. According to Fig. 3a, YS shows a linear relationship with the logarithm of strain rate for all the alloys. It is found that the YS of Ti-4733 increases considerably with strain rate and increases from 830 MPa at 7×10^{-5} s^{-1} to 923 MPa at 7×10^{-2} s^{-1}, while the YS of Ti-3873 shows a slight variation with strain rate and only increased from 1010 MPa at 7×10^{-5} s^{-1} to 1020 MPa at 7×10^{-2} s^{-1}. In the case of Ti-3573, YS increases with increasing strain rate, but the amount is intermediate between those of Ti-3873 and Ti-4733. Fig. 3b shows that in contrast to YS, the n value of Ti-4733 is almost independent of strain rate while the n value of Ti-3873 is quite sensitive to it during compression.

The third parameter, the SRS of the flow stress, m value of the alloys, calculated according to Eq. (2), was also determined and plotted in Fig. 3c as a function of true strain.

$$m = \frac{\partial(\log \sigma)}{\partial(\log \dot{\varepsilon})} \tag{2}$$

where m is SRS factor, σ is the true stress and $\dot{\varepsilon}$ is strain rate. It is seen that with increasing the stability, the alloys exhibit lower SRS. Furthermore, the SRSs of Ti-4733 and Ti-3573 are almost constant over the strain range studied here, the very low SRS of Ti-3873 increases significantly with increasing the applied strain. This suggests that some change occurs in deformation behavior of Ti-3873 during compression.

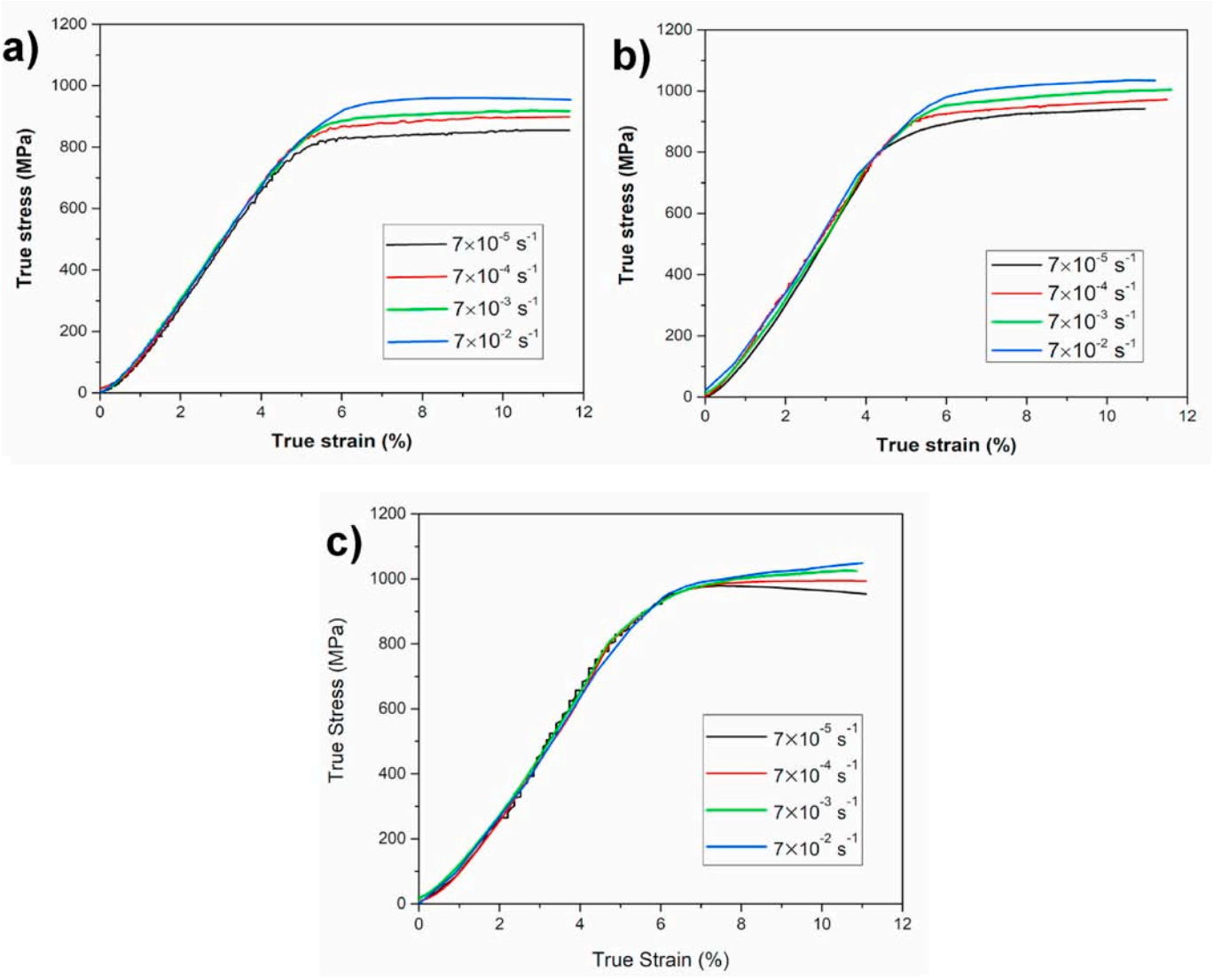

Fig. 2. Compressive true stress-true strain curves of the alloys at different strain rates. (a) Ti-4733, (b) Ti-3573 and (c) Ti-3873.

3.3. *Deformation structure evolution in the lowest stability alloy Ti-4733*

Figs. 4 and 5 show examples of laser scanning and EBSD micrographs, respectively, of Ti-4733 deformed at the lowest and highest strain rates of 7×10^{-5} and 7×10^{-2} s^{-1}. Different types of deformation features including some thin parallel plates and some polyline or wavy thin lines were observed in the samples deformed at the low strain rate of 7×10^{-5} s^{-1} as shown in Fig. 4a. Fig. 4b and c displays a higher magnification of these two deformation features which are probably DIM and slip lines. EBSD scans were used for a better understanding of the nature of these deformation features. According to Fig. 5a and b, the inverse pole figure (IPF) and phase maps of the deformed Ti-4733 show the presence of few martensite bands which naturally are not perfectly indexed. This has also been reported by some other researchers [23]. The occurrence of orthorhombic α" martensite is confirmed by an XRD patterns of the deformed sample as shown in Fig. 4e. In addition to DIM, several thin lines are observed in the image quality (IQ) map of Ti-4733 in Fig. 5c. As these lines are invisible in the IPF map, it can be concluded that these lines do not represent significant misorientation or different crystal structures and therefore they are most probably slip lines. Based on these observations, the DIM transformation and dislocation slip can be identified as the active deformation mechanisms in Ti-4733 at the low strain rate, as previously reported elsewhere [14] as well.

As the laser scanning image of the microstructure of the specimen deformed at the high strain rate of 7×10^{-2} s^{-1} illustrates (Fig. 4d), the number fraction of deformation products increases significantly, while according to XRD results (not shown here) and previous studies [12,13] the volume fraction of DIM does not change significantly (fraction less than 5%) with increasing the strain rate. The EBSD scans of the same specimen are presented in Fig. 6. According to the IPF map, most of the deformation products are slip lines. However, in addition to slip lines, there are some bands with different orientation from the matrix which were identified to have the same BCC crystal structure as the matrix had. The kernel average misorientation (KAM) map of the sample in Fig. 6c reveals that a high density of geometrically necessary dislocations exists within the bands. Fig. 6e shows the variation of misorientation angle along the line drawn across the band in Fig. 6d. As seen, the misorientation angle is below 30° and also changes along the line. This indicates that these bands cannot be twins or martensite phase and are most probably local deformation bands, which usually form during deformation at high strain rates [9].

3.4. *Deformation structure evolution in the intermediate stability alloy Ti-3573*

Regarding Ti-3573 with the intermediate stability, several relatively

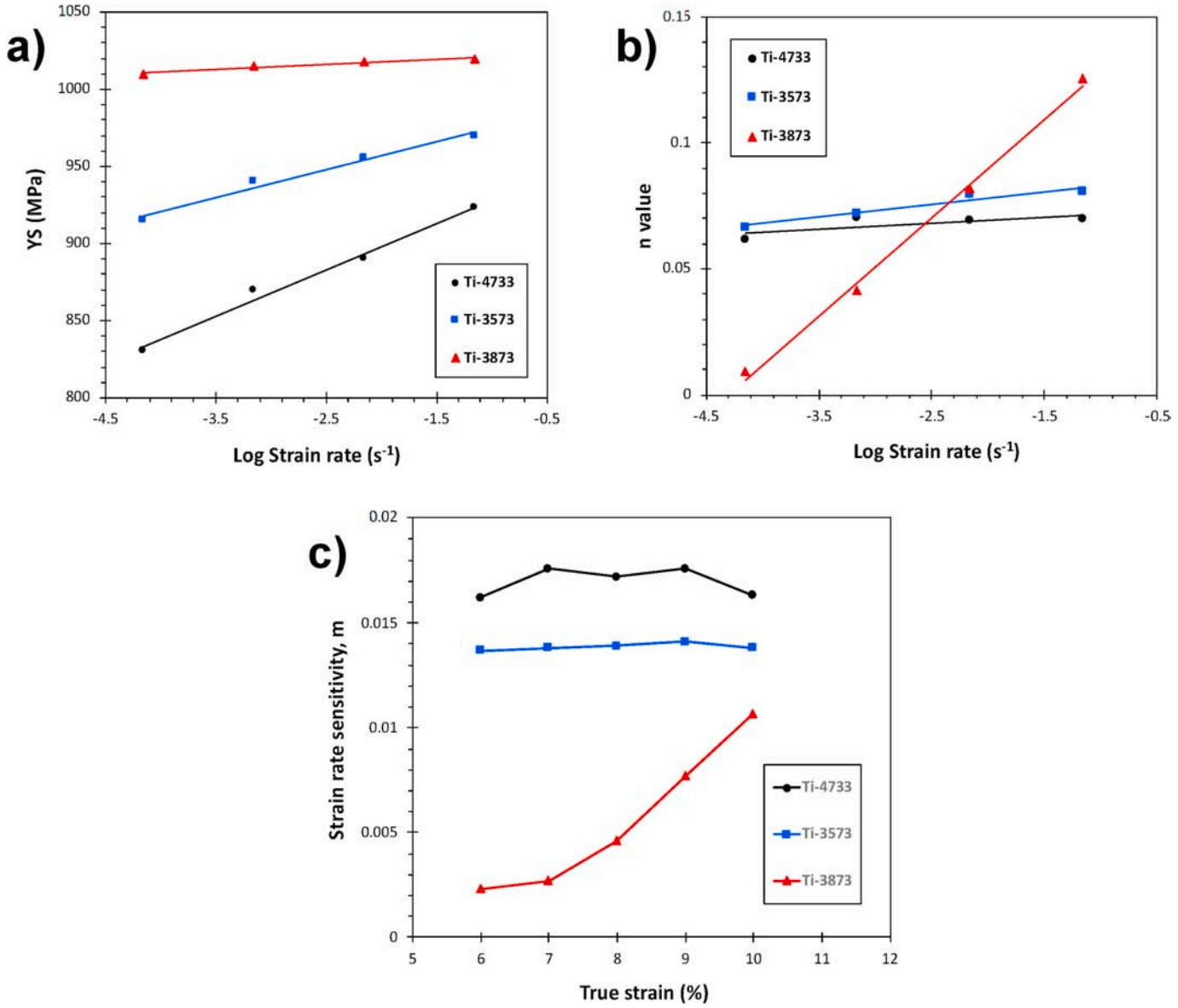

Fig. 3. Variation of (a) yield strength (YS) and (b) strain hardening exponent (n) as a function of strain rate and (c) variation of strain rate sensitivity factor (m) with true strain.

wide bands with straight and parallel boundaries were also observed in addition to DIM and slip lines, as shown in Fig. 7a and b. Fig. 8 displays the EBSD map after 10% compressive strain containing some of those wide deformation bands in the beta matrix. The IPF map in Fig. 8b shows that these bands have a same crystal structure as the matrix has and they possess a constant misorientation angle of 50.5° (Fig. 8c) which is the characteristic of {332} <113> twinning system in beta Ti alloys [5,24]. Therefore, the misorientation profile in Fig. 8c evidences that the wide deformation bands displayed in Fig. 7 are {332} <113> twins. The phase map shown in Fig. 8d reveals that some martensite can also be identified inside the twins indicating that DIM formation is also an active deformation mechanism. Therefore, it can be concluded that deformation mechanism of Ti-3573 is a combination of dislocation slip, twinning and DIM formation at the low strain rate of $7 \times 10^{-5}\ s^{-1}$. With increasing the strain rate, it is noticed from Fig. 7c and d that there is no significant change in the number fraction of twins while the number of slip lines increased. This is in agreement with the results of Ji et al. [15] who reported a very slight increase in the twinning fraction up to the tensile strain of 10%. The EBSD scans of the sample deformed at the high strain rate of $7 \times 10^{-2}\ s^{-1}$ reveal that with increasing strain rate, some new martensite and deformation bands were formed in addition to increased number of slip lines and twins as seen in Fig. 9. This means that the deformation mechanism of Ti-3573 which is a combination of martensite formation, twinning and dislocation slip at $7 \times 10^{-5}\ s^{-1}$ does not change with increasing the strain rate and only the fractions of slip lines and martensite increase without considerable increase in the twin fraction. This is in agreement with the results of Zhan et al. [8], who showed that in a beta Ti alloy with deformation mechanism of DIM, twinning and dislocation slip, the volume fraction of twins remains almost constant independent of strain rate.

Since a combination of multiple mechanisms is simultaneously active in Ti-3573, recognizing the effect of strain rate on each mechanism is not easy and needs more studies. However, the overall effect of strain rate on mechanical behavior of this alloy is something between those of Ti-4733 and Ti-3873. It is worth mentioning that as the amount of DIM is so low in this alloy, twinning can be considered as the dominant mechanism.

3.5. *Deformation structure evolution in the high stability alloy Ti-3873*

In the case of Ti-3873, the highest stability among the studied alloys,

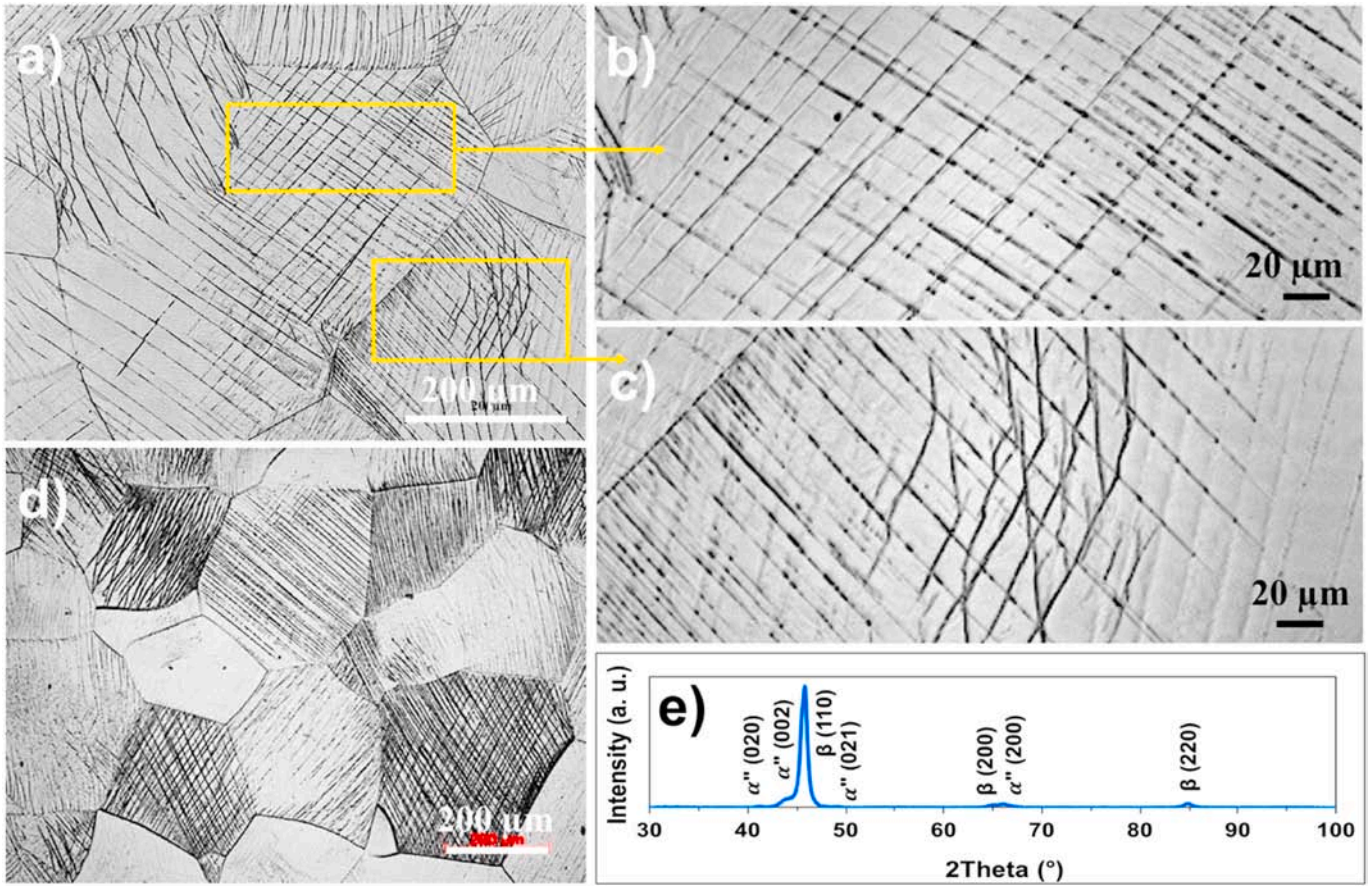

Fig. 4. Laser optical micrographs of the samples after 10% strain at the strain rates of: (a), (b), (c) 7×10^{-5} s^{-1} and (d) 7×10^{-2} s^{-1}. XRD pattern corresponding to the sample deformed at 7×10^{-5} s^{-1}(e).

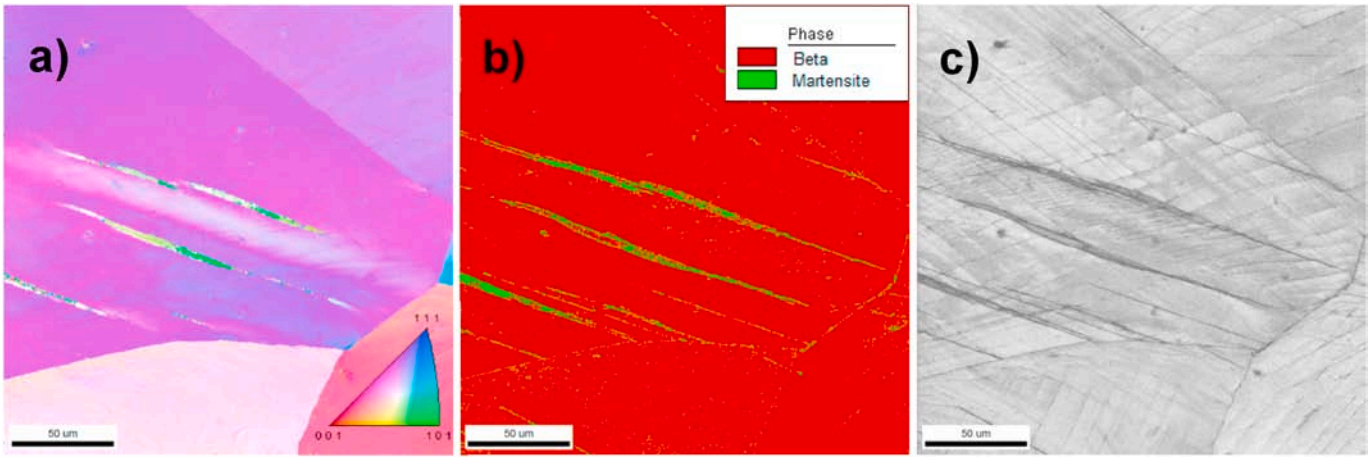

Fig. 5. EBSD maps of Ti-4733 after 10% strain at the strain rate of 7×10^{-5} s^{-1}. (a) Inverse pole figure (IPF), (b) phase map and (c) image quality (IQ) map.

Fig. 10 indicates that there are no deformation bands or twins in the microstructure of the sample deformed to 10% strain at the low strain rate of 7×10^{-5} s^{-1} and the vast majority of deformation products are slip lines. The IPF map, displayed in Fig. 11, also confirms this observation. In addition, the XRD pattern in Fig. 11c only shows peaks corresponding to the beta phase but no α" martensite peaks are visible. This means that the martensite start temperature of Ti-3873 is well below room temperature. Therefore, it can be concluded that the deformation mechanism of Ti-3873 is dislocation slip at the low strain rate of 7×10^{-5} s^{-1}.

With increasing the strain rate to 7×10^{-2} s^{-1} a significant increase in the number of slip lines occurred, as seen in Fig. 12. In addition to this, some thick bands were also visible in the microstructure after deforming at this high strain rate (Fig. 12a and b). The IPF map of the corresponding microstructure, depicted in Fig. 13, revealed that those thick band are actually {332} <113> twins. This means that increasing strain rate from 7×10^{-5} s^{-1} to 7×10^{-2} s^{-1} led to a change in deformation mechanism from sole slip to a combination of dislocation slip and twinning.

It was also noticed that in contrast to Ti-4733 where the slip lines

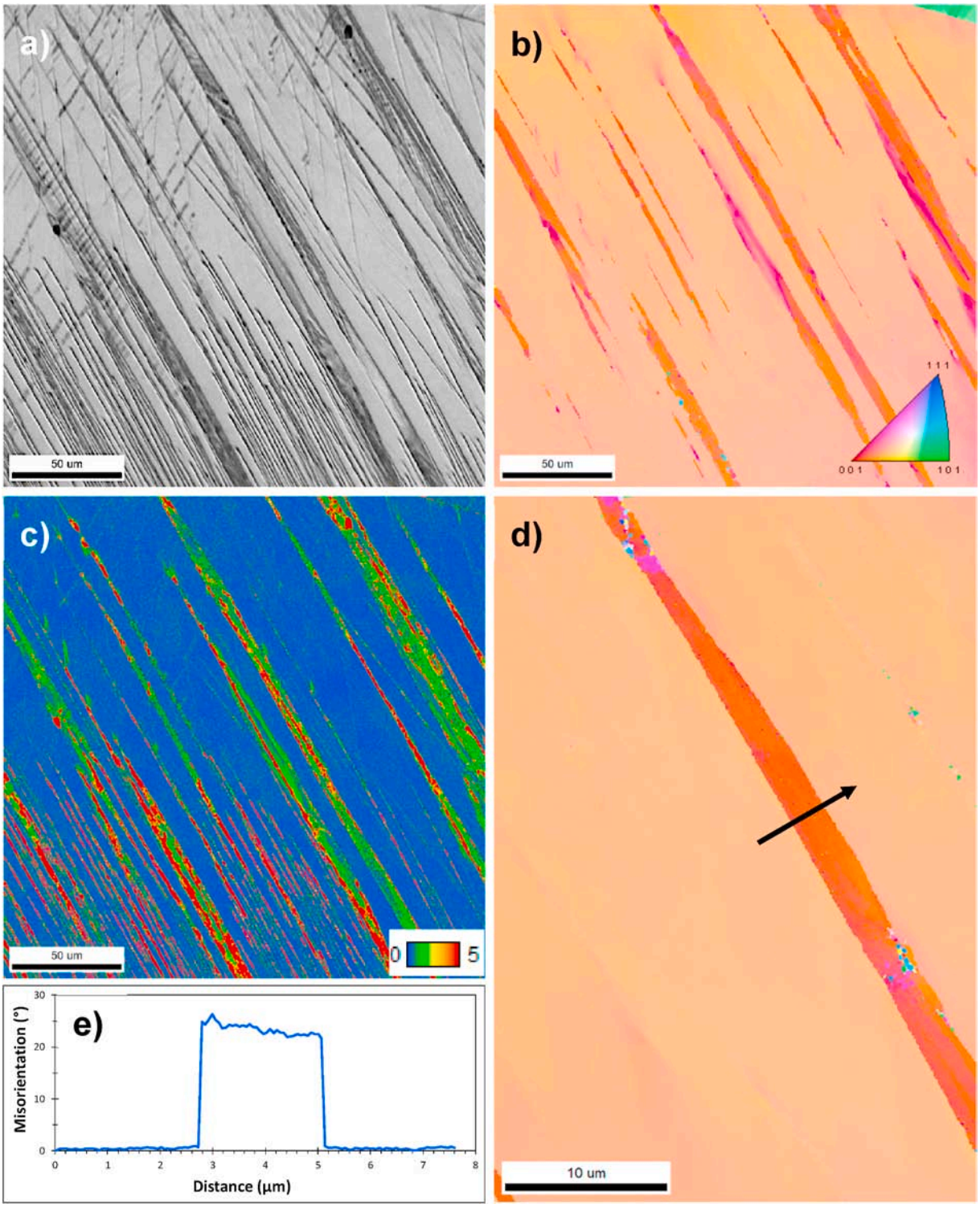

Fig. 6. EBSD maps of Ti-4733 after 10% strain at strain rate of $7 \times 10^{-2}\ s^{-1}$. (a) Image quality (IQ), (b) inverse pole figure (IPF) and (c) kernel average misorientation (KAM) map. (d) High magnification IPF map of a deformation band and (e) misorientation angle variation along the black arrow shown in (d).

were mostly in the same direction (Fig. 4d), slip lines in Ti-3873 deformed at the high strain rate were mainly multi-directional (Fig. 12c) corresponding to the occurrence of cross slip. Even though slip lines were observed in all the alloys, Ti-3873 exhibited a higher number density of slip lines and a higher frequency of cross slip indicating that cross slip was more extensive in Ti-3873. This can be attributed to the high stability of Ti-3873, resulting in a higher critical resolved shear stress (CRSS) for dislocation slip. The high CRSS prevents the formation of easy paths for dislocation slip, and as a result, multiple slip systems with sufficiently high Schmid factors are activated which leads to increased intensity of cross slip.

4. Discussion

Analyses of compression flow curves and microstructural observations indicated that different deformation mechanisms were activated in

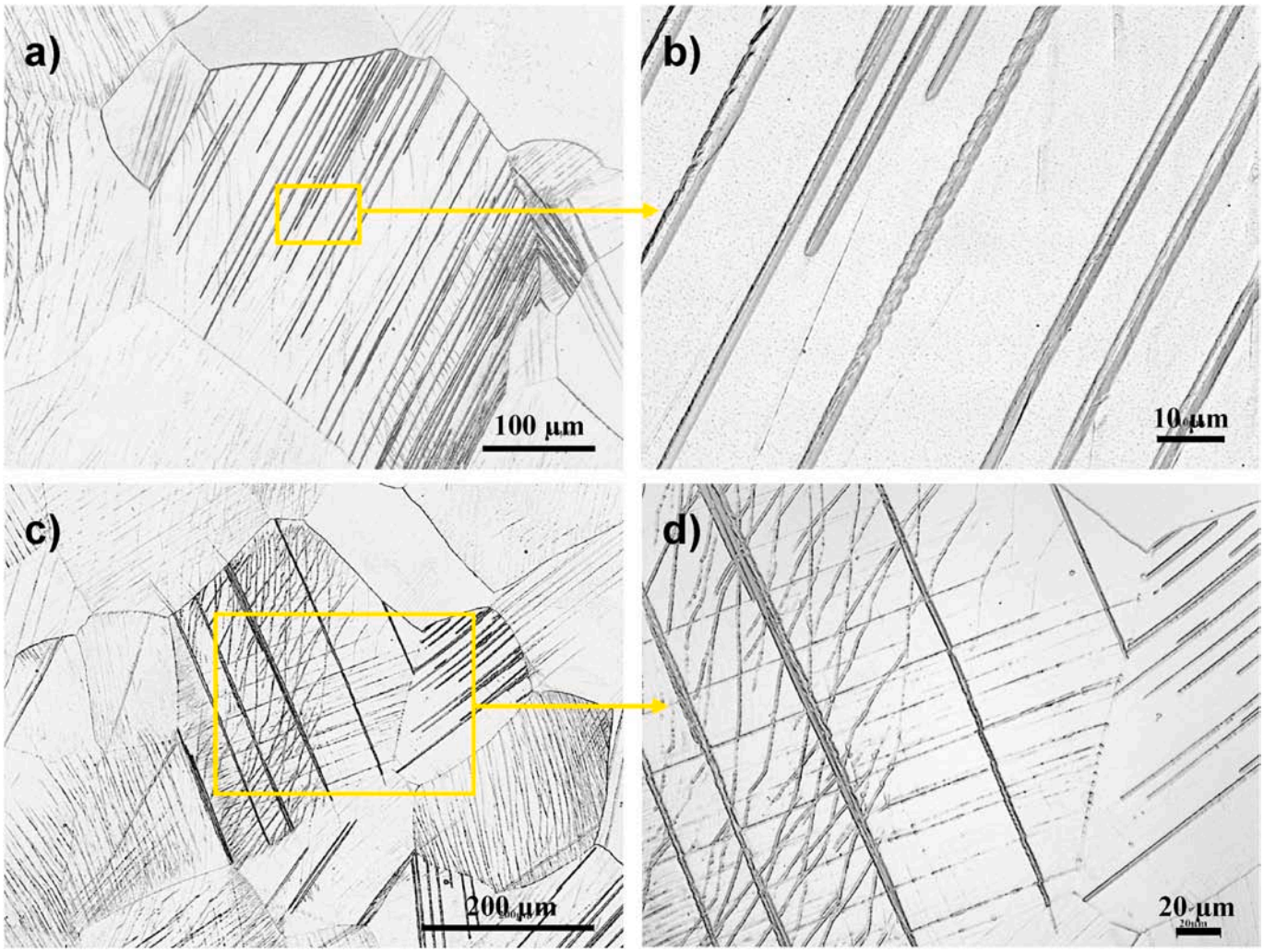

Fig. 7. Laser scanning micrographs of Ti-3573 after 10% strain at the strain rates of: (a and b) 7×10^{-5} s^{-1} and (c and d) 7×10^{-2} s^{-1}.

the studied three alloys and consequently effects of the strain rate on the YS, strain hardening and SRS also vary. The results are briefly discussed.

4.1. Yield strength

The difference of the atomic size of an alloying element compared with the Ti atom size might be a simple factor affecting the YS of annealed solid solution. According to Ref. [25], the atom sizes are Ti 176 p.m., Mo 190 p.m., V 171 p.m., Cr 166 p.m., and Al 118 p.m., suggesting the highest influence of Al and Mo. However, the following equation has been suggested for estimating the solid solution strengthening ($\Delta\sigma$) of alloying elements in single beta phase Ti alloys [18]:

$$\Delta\sigma = f\,[1.5(Fe + Mn) + 1.3(Cr) + (Al + Mo) + 0.7(V + W) + 0.5(Sn) + 0.4(Zr) + 0.3(Nb)] \quad (3)$$

where f is a constant between 40 and 50 MPa and the elements are in weight percent (wt.%). Based on Eq. (3), YS was calculated to be in the range of 680–850 MPa for Ti-4733, 672–840 MPa for Ti-3573 and 792–990 for Ti-3873, i.e. quite similar for the low and intermediate stability alloys, but distinctly higher for the high stability alloy. This is consistent with the measured results (Fig. 2).

As seen in Fig. 3a, the YS increased with increasing strain rate, but the effect became smaller with increasing the stability of beta phase. This must be a result from the chemical composition of the alloys, for plastic deformation is minor yet for the 0.2% strain offset YS, and the deformation mechanisms appearing with further strain cannot affect it. The background of the SRS is in the thermal component of the flow stress, where the probability of dislocations to overcome obstacles on glide planes depends on time, and thermal activation remains less at high strain rates [26]. Thus, we may conclude that especially the athermal component (non-dislocation dominant) of the YS has increased by the alloying providing higher stability.

In the strain rate range studied in the present work (7×10^{-5} to 7×10^{-1} s^{-1}), most BCC metals including beta Ti alloys exhibit a linear increase in YS with logarithm of strain rate. For example, according to Li et al. [13] the YS of Ti–10V–2Fe–3Al alloy increased linearly this way from about 650 MPa at 10^{-4} s^{-1} to 740 MPa at 10^{-1} s^{-1}. This SRS of YS is similar to that of Ti-4733 and interestingly both the alloys exhibit similar level of stability based on Mo_{eq}.

4.2. Deformation mechanisms

From microstructure evolutions it can be noticed that the strain rate affected the deformation mechanisms differently in the studied alloys. As evident from Figs. 4 and 6, no significant change in the nature and number density of deformation features, DIM and slip lines, occurred in the lowest stability Ti-4733 alloy with changing the strain rate, whereas in the intermediate stability Ti-3573 alloy, the number density of twins and DIM laths slightly increased, though the type of deformation features remained unchanged. However, in the highest stability Ti-3873 alloy, not only the number density of deformation features increased significantly at the higher strain rate, but also the nature of features

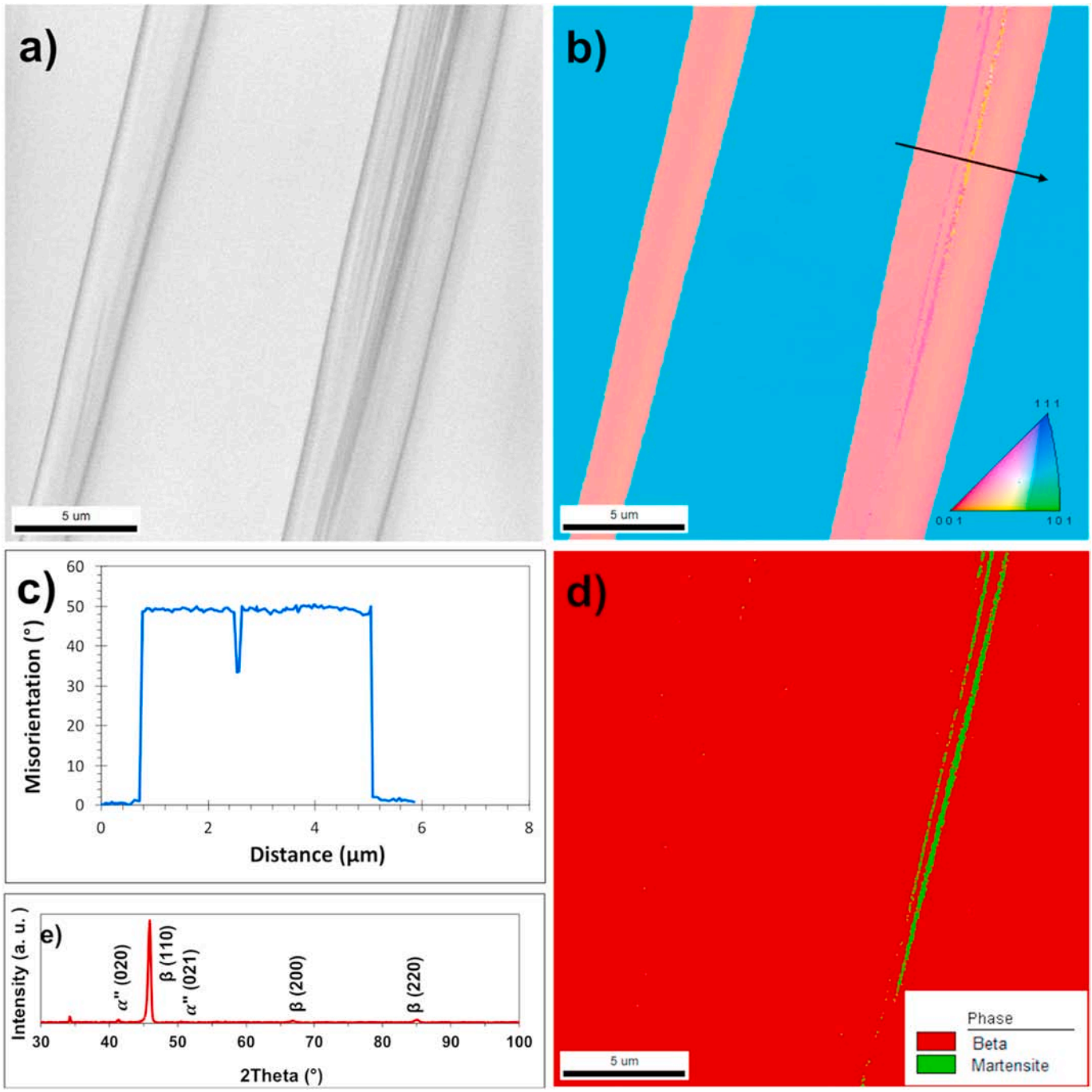

Fig. 8. EBSD maps of the sample after 10% strain at the strain rate of 7×10^{-5} s^{-1}. (a) IQ map, (b) IPF map, (c) misorientation angle along the arrow shown in (b), (d) phase map and (e) corresponding XRD pattern of the sample showing some weak α" martensite peaks.

changed so that also numerous {332} <113> twins existed in the deformed structure. Zhou and Chew [27] reported the change in deformation mechanism from dislocation slip at low strain rates to twinning at the high strain rate for a Ti–6Al–4V alloy. The CRSS required for DIM and twinning is usually less than that of dislocation slip at room temperature in Ti alloys [28]. The CRSS of twinning is independent of strain rate because of non-diffusional nature of twinning [29], whereas for DIM it has been shown that CRSS increases with the logarithm of strain rate [12,14]. According to the thermo-statistical model presented by Calindo Nava and Rivera-Díaz-del-Castillo [30], the number of dislocations required for nucleation of a twin is proportional to the number of dislocations in dislocation forest. Therefore, it can be concluded that a higher number of dislocations may activate nucleation of a higher number of twins. Regarding the effect of strain rate on twinning, the increased strain rate increases dislocation density and accelerates their movement. Given that the critical shear stress for twinning is independent of strain rate [29], increasing strain rate results in the nucleation of a higher number of twins. Therefore, it is expected that the number fraction of twins increases with increasing strain rate, and this is seen in the present qualitative results for Ti-3873. Similar results have been reported by Ahmed et al. [16] for a beta Ti–10V–3Fe–3Al-0.27O (wt.%) alloy containing alpha and omega phases which exhibited TRIP/TWIP effect. Also, in commercial pure alpha Ti the fraction of twins has been reported to increase with increasing the strain rate [31]. Ji et al. [15] found that, in a Ti–10Mo–1Fe alloy showing the TWIP effect, tensile deformation at a higher strain rate (difference of four orders of

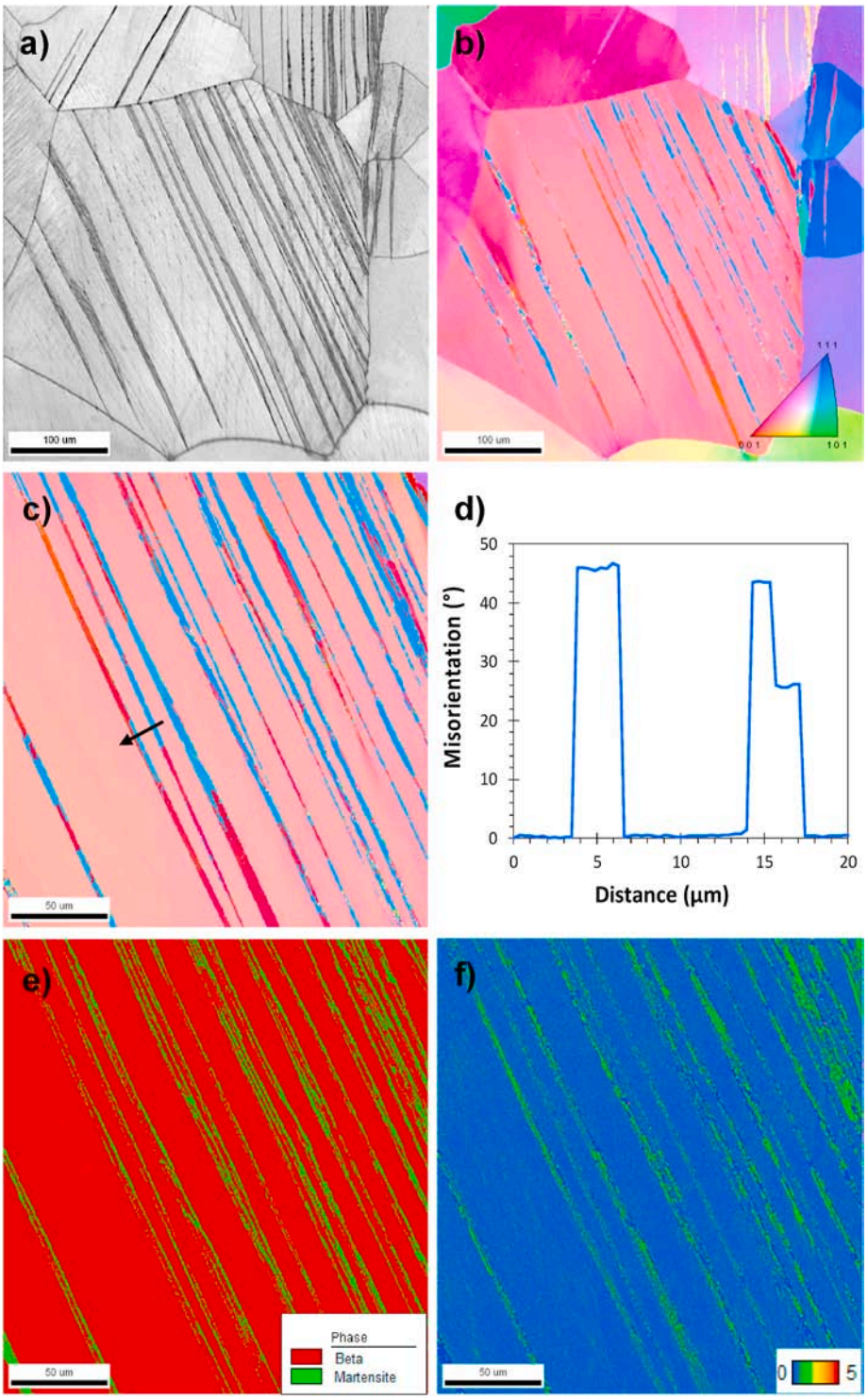

Fig. 9. EBSD maps of the Ti-3573 sample after 10% strain at the strain rate of 7×10^{-2} s^{-1}. (a) IQ, (b) IPF maps, (c) higher magnification IPF map of the area shown with a rectangle in (a), (d) misorientation angle along the arrow shown in (b), corresponding (e) phase map and (f) KAM map of (c).

magnitude) resulted in higher twin fraction at strains smaller than 5%, but in a lower fraction at strains higher than 10%, though the difference was small (less than 8% at the strain of 14%). They thought the nucleation and growth of twins are retarded at the higher strain rate deformation, leading to a lower area fraction of twins. However, this only occurs when the strain exceeds a certain level and a smaller rate of increasing dislocation density is observed at higher strain rate.

4.3. Strain hardening exponent, n value

As depicted in Fig. 3b, the n value is very low when the deformation mechanism is solely dislocation slip as that in Ti-3873 at low strain rates. Usually, the n value of metals and alloys with BCC and HCP crystal structures is very low. For instance, the low value of 0.05 has been reported for Fe [32]. Similarly, very low n values of about 0.038, 0.04 and 0.06 have been reported for alpha-beta Ti–6Al–4V, Ti-6242 and Ti-834 alloys [33]. Song et al. [34] presented a higher n value of 0.11 for a

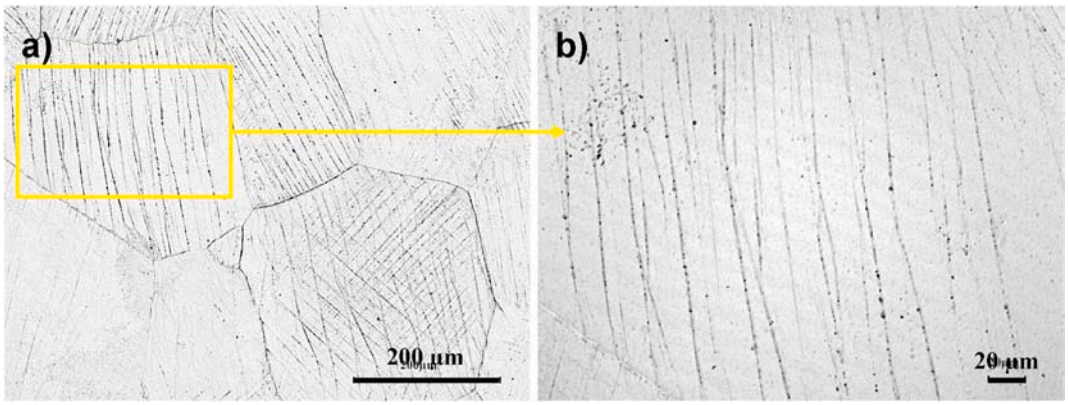

Fig. 10. Laser optical micrographs of a Ti-3873 sample after 10% strain at the strain rate of 7×10^{-5} s^{-1}.

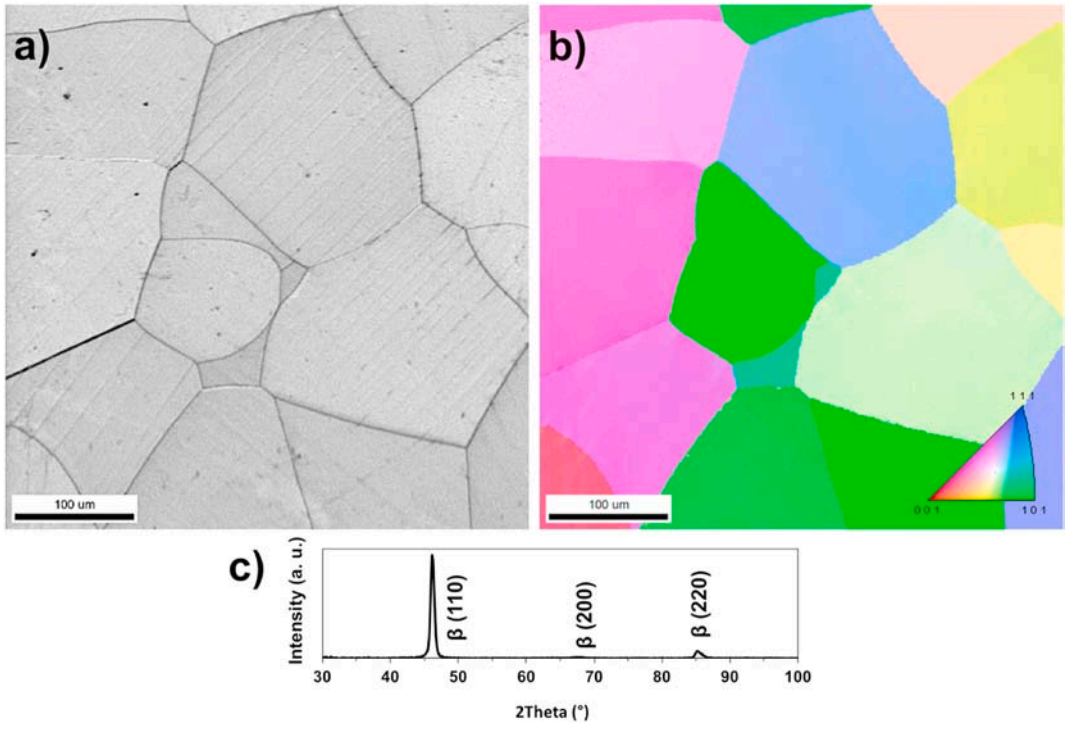

Fig. 11. EBSD maps of a sample deformed to 10% strain at the strain rate of 7×10^{-5} s^{-1} (a) IQ and (b) IPF map. (c) XRD pattern of the corresponding sample.

metastable beta Ti alloy showing DIM formation. The different deformation mechanisms can lead to different strain hardening behavior and SRS of the flow stress.

In the present experiments, it was observed that the variation of n with the strain rate was insignificant for Ti-4733 (Fig. 3b), which can be attributed to the same deformation mechanism at all strain rates applied. This value of n (≈0.07) is quite low. While in metastable austenitic steels, adiabatic heating created at high strain rates can affect the stability of austenite matrix against martensitic transformation and lead to a change in deformation mechanism [35,36], it has been shown that the temperature rise is not significant (<40 °C) in beta Ti alloys with respect to true strain up to ~10% at strain rates in a range similar to the present work [13,15].

In the case of Ti-3573 showing a combination of TRIP and TWIP effects, even though no change in the deformation mechanism with strain rate, the increased number of twins resulted in a slight increase of n (≈0.07 to 0.08). Zhan et al. [8] found insignificant influence of strain rate varying by six orders of magnitude on strain hardening of a Ti–25Nb–3Zr3Mo–2Sn alloy showing multiple deformation mechanisms including formation of two types of twins. Anyhow, n ~ 0.23 was distinctly higher than n values for the present alloys.

However, in Ti-3873, the change in the dominant deformation mechanism from dislocation slip to mechanical twinning led to a sharp increase in n value from 0.01 to 0.13. The n value usually decreases with increasing the strain rate due to the increasing number of dislocation pile-ups. However, in the case that some obstacles such as threshold amount of dislocations or twin or phase boundaries are already present decreasing the mobility of dislocations, an opposite trend may be observed. For example, Gupta et al. [37] reported that when 10–15% prior cold work was applied to a Ti–6Al–4V, where sufficient number of dislocation pile ups was present, n value was seen to increase with the strain rate. Tsao et al. [38] showed that the n value of a CP-Ti sheet increased with increasing strain rate due to increase of dislocation density and dislocation multiplication rate. Regarding Ti-3873, it can be supposed that similar enhanced hardening can occur when twin boundaries are dynamically created during deformation.

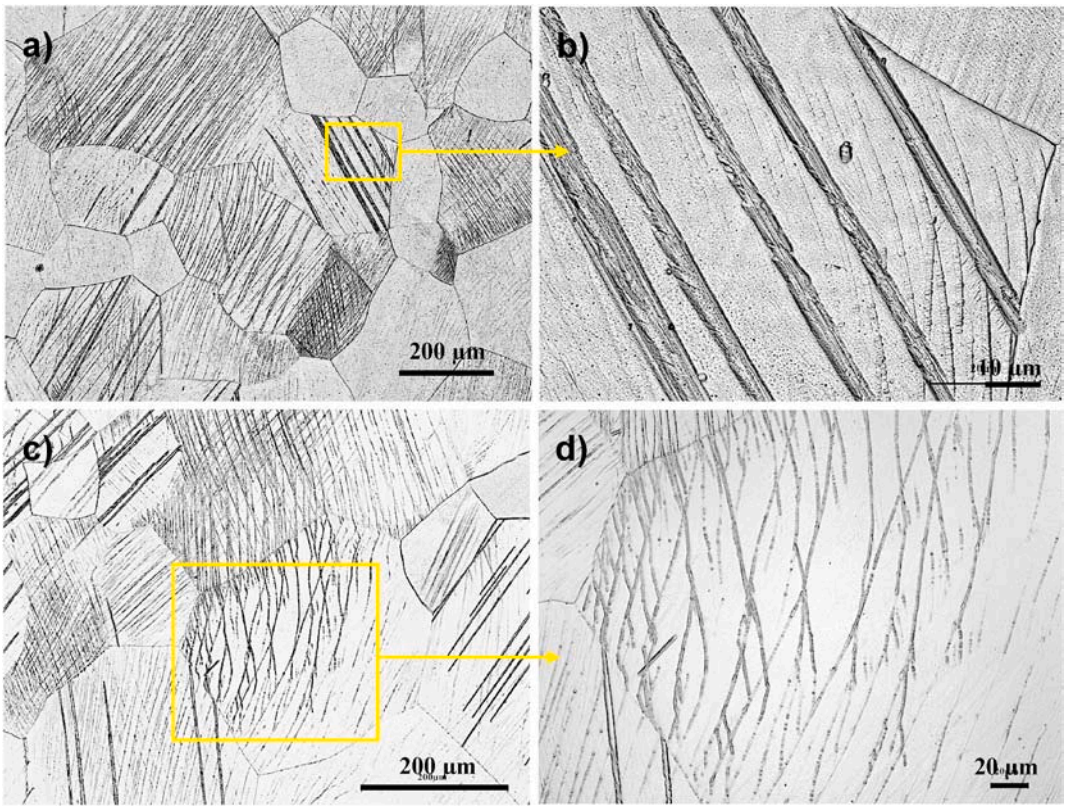

Fig. 12. Laser optical micrographs of samples after 10% strain at the strain rate of 7×10^{-2} s^{-1}. (a) and (b) twins and (c) and (d) cross-slip lines.

4.4. Strain rate sensitivity, m value

Positive and high m value is important to prevent local necking and thereby enhancing the ductility. Ji et al. [15] found negative m values for a Ti–10Mo–1Fe alloy at strains higher than 0.13. All the present alloys exhibited a positive m value in the studied strain range. In general, alloys with BCC structures including beta Ti alloys exhibit a higher m value compared to those with FCC structure [39]. For example, the m value of large-grained Cu is around 0.004 at room temperature [39]. The m value for the commercial beta Ti alloys of Ti-15-3, Beta C and TIMETAL 21S has been reported to be around 0.008 [40], which is much lower value than that observed for the present Ti-4733 and Ti-3573 alloys.

The stability of an alloy can be a factor affecting its m value. According to Fig. 3c, m decreased with increasing the mechanical stability of the present alloys from Ti-4733 to Ti-3573 and then to Ti-3873. Thus, the low m value of the above commercial alloys can be due to their high stability. A higher m value of 0.016 has been reported for Beta III [40] which is quite close to that of Ti-4733 and Ti-3573. Wang et al. [41] have demonstrated that in Ti-xAl-yMo-zV alloys, increasing Mo content (i.e. increasing the beta phase stability) results in a decrease of m value. They showed that under multiple slip deformation conditions increasing the Mo content promotes screw dislocation pinning by the mechanism of super-jog formation. It has been shown that these super-jogs act as strong pinning points for screw dislocations at high solute concentrations [42] and may lead to a decrease in SRS.

As illustrated in Fig. 3c, the m value of Ti-4733 and Ti-3573 was found to be almost constant in the ranges of 0.013–0.014 and 0.016–0.018, respectively, while that of Ti-3873 increased from very small value of 0.001 up to 0.011. This is in contrast with previous results of Ji et al. [15], where m values decreasing with strain were found for a Ti–10Mo–1Fe alloy. However, it has been very recently shown [43] that the alpha-beta alloys of Ti-6246 and Ti-64 exhibit an increasing m value with strain until the saturation values of 0.007 and 0.01, respectively. It has been reported that the deformation mechanism of beta Ti alloys is related not only to the beta phase stability, but also to the extent of plastic deformation [44]. Though that the effect of strain on the deformation mechanism was not investigated in the present study, the deformation mechanism might alter with increasing strain and result in a change in SRS (m value). It is known that in Ti alloys showing DIM formation, martensite is formed by stress induced [45,46], so in Ti-4733, no slip precedes DIM formation. However, in Ti-3873 the dislocation slip may occur before the onset of twinning at high strain rates, so that the initial low m value would be related to the higher content of alloying elements like Mo (i.e. the high stability) while the following increase in the m value might correlate with the activation of twinning with increasing strain. However, detailed observations are needed to understand how the extent of strain affects the evolution of deformation mechanisms.

4.5. Stability-strain rate-mechanism (SSM) diagram

Fig. 14 summarizes schematically the effect of beta phase stability, predicted based on the Mo_{eq} parameter, and strain rate on determining the deformation mechanism in the studied alloys along with several beta Ti alloys from literature. According to this stability-strain rate-mechanism (SSM) diagram, with increasing the stability the deformation mechanism changes from DIM formation to twinning and then to slip band (SB) formation at the low strain rate of 7×10^{-5} s^{-1}. Furthermore, the SSM diagram indicates that with increasing the strain rate to 7×10^{-2} s^{-1}, the deformation mechanism changes from DIM to SB formation in Ti-4733, remains unchanged in Ti-3573 and changes from SB to mechanical twinning in Ti-3873. It is worth noting that the possible influence of the strain rate is not taken into account in the stability parameters listed in Table 2 (or in the $\overline{Bo}$-$\overline{Md}$ map in Fig. 1a). However, the present experimental results demonstrate that the deformation mechanisms, i.e. the mechanical stability of the beta phase, is affected by the strain rate, so that the area corresponding to the TWIP effect is

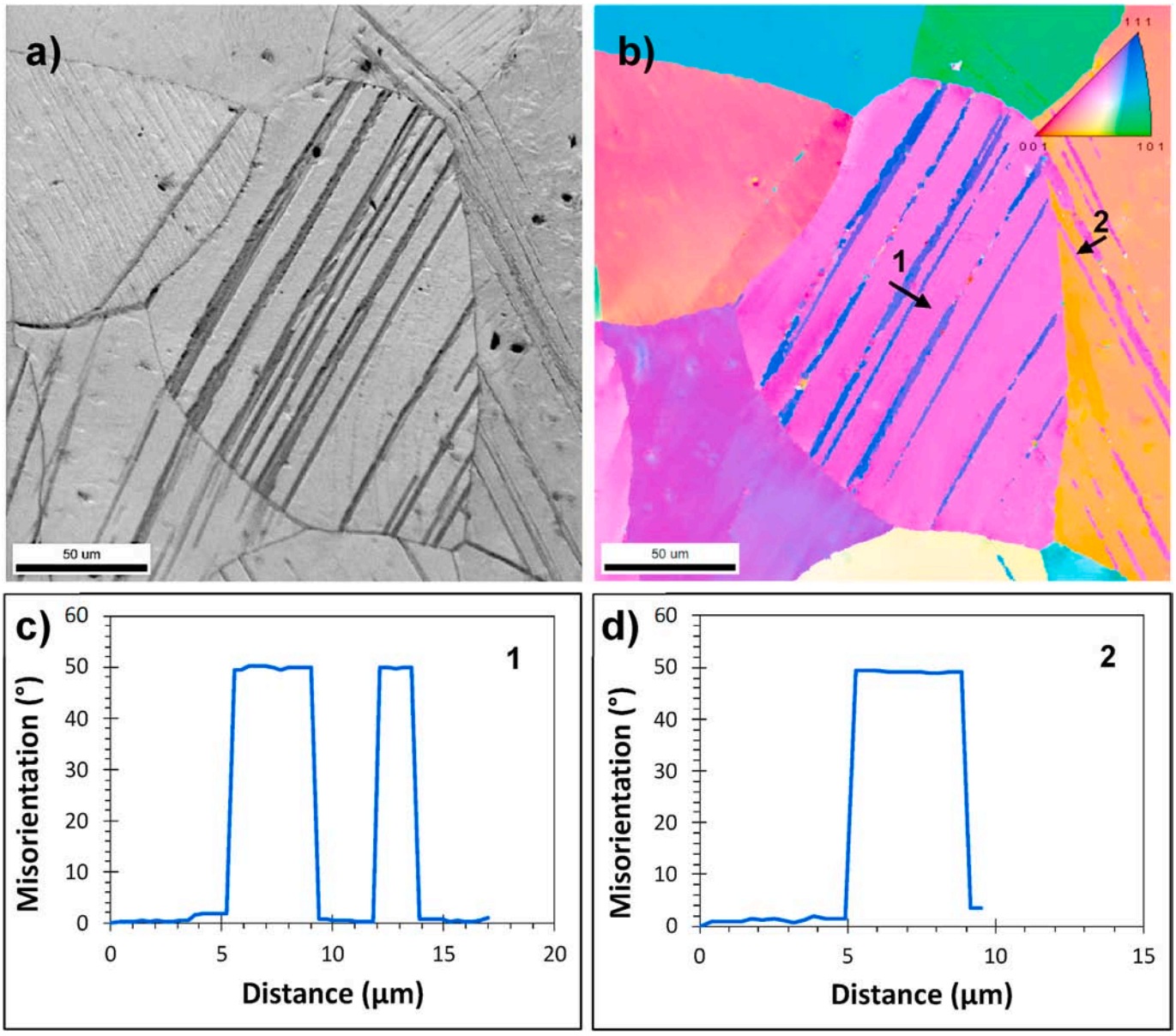

Fig. 13. EBSD maps of the sample deformed at the strain rate of 7×10^{-2} s^{-1}, (a) IQ map and (b) IPF map. Misorientation angle along the arrows 1 (c) and 2 (d) shown in (b).

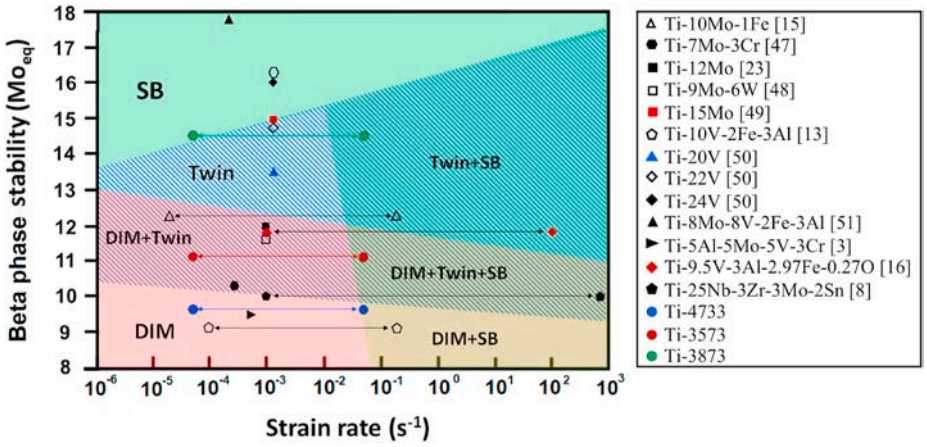

Fig. 14. Schematic diagram showing the effect of beta phase stability and strain rate on determining the active deformation mechanisms DIM, twin and slip band (SB) formation in various beta Ti alloys [3,8,13,15,16,23,47–51].

expanded with increasing the strain rate. According to the SSM diagram, at high levels of stability the mechanical stability decreases with increasing the strain rate while it increases with increasing the strain rate at low levels of stability. For example, with increasing the strain rate the deformation mechanism of high-stability Ti-3873 changes from simple dislocation slip (SB) to twinning which is the mechanism of the alloys with a lower stability. But for a low-stability Ti-4733 alloy, the mechanism changes from DIM to DIM + SB, i.e. to the mechanism of alloys with a higher stability. It should be mentioned that the borders in the SSM diagram shown in Fig. 14 are drawn based on available data from literature and more experiments are needed to determine the exact positions of them. In addition, as it was mentioned before, increasing the strain value may affect deformation mechanisms, i.e. the beta phase stability, so this should also be considered in using the SSM diagram. However, we believe that the SSM diagram can provide a useful complement to the $\overline{Bo}$-$\overline{Md}$ diagram in predicting the deformation mechanism of beta Ti alloys.

5. Summary

The effect of strain rate in 10% compression deformation at room temperature on the deformation mechanisms martensite (DIM) formation, twinning and dislocation slip were investigated in three beta Ti alloys possessing different stability.

1) The YS of the alloys increased and its sensitivity to strain rate decreased with increasing the stability.
2) Deformation mechanisms varied depending on the stability and also strain rate. Deformation mechanism could also change during straining.
3) The strain hardening exponent (n value) only increased slightly with increasing the strain rate for the alloys with the lowest and intermediate stability but significantly for the highest stability alloy. This was attributed to the change in deformation mechanism of the highest stability alloy from dislocation slip to mechanical twinning with increasing strain rate.
4) The strain rate sensitivity factor (m-value) decreased with increasing the beta phase stability. It remained almost constant over the studied strain range for alloys with the low and intermediate stability, but it was very low for the highest stability alloy although increased significantly with increasing the applied strain.
5) Based on the room temperature compression tests on three beta Ti alloys with different levels of mechanical stability and at four strain rates (difference of three orders of magnitude), the stability-strain rate-mechanism (SSM) diagram was introduced to utilize as the complement of a $\overline{Bo}$-$\overline{Md}$ diagram for predicting the deformation mechanisms of beta Ti alloys.

Data availability statement

The raw/processed data required to reproduce these findings cannot be shared at this time as the data also forms part of an ongoing study.

CRediT authorship contribution statement

S. Sadeghpour: Conceptualization, Investigation, Formal analysis, Visualization, Writing - original draft, Writing - review & editing. **V. Javaheri:** Formal analysis, Visualization, Writing - review & editing. **S. Bruschi:** Validation, Writing - review & editing. **J. Kömi:** Supervision, Project administration. **P. Karjalainen:** Formal analysis, Validation, Writing - review & editing, Supervision.

Declaration of competing interest

The authors declare that they have no known competing financial interests or personal relationships that could have appeared to influence the work reported in this paper.

Acknowledgments

The authors are grateful for financial support from Academy of Finland (#311934 - Genome of Steel Project).

References

[1] S. Sadeghpour, S.M. Abbasi, M. Morakabati, S. Bruschi, Correlation between alpha phase morphology and tensile properties of a new beta titanium alloy, Mater. Des. 121 (2017) 24–35, https://doi.org/10.1016/j.matdes.2017.02.043.
[2] D. Banerjee, J.C. Williams, Perspectives on titanium science and technology, Acta Mater. 61 (2013) 844–879, https://doi.org/10.1016/j.actamat.2012.10.043.
[3] S. Sadeghpour, S.M. Abbasi, M. Morakabati, A. Kisko, L.P. Karjalainen, D.A. Porter, On the compressive deformation behavior of new beta titanium alloys designed by d-electron method, J. Alloys Compd. 746 (2018) 206–217, https://doi.org/10.1016/j.jallcom.2018.02.212.
[4] H. Ohyama, T. Nishimura, Effects of alloying elements on deformation mode in Ti-V based β titanium alloy system, ISIJ Int. 35 (1995) 927–936, https://doi.org/10.2355/isijinternational.35.927.
[5] S. Hanada, O. Izumi, Transmission electron microscopic observations of mechanical twinning in metastable beta titanium alloys, Metall. Trans. A. 17 (1986) 1409–1420, https://doi.org/10.1007/BF02650122.
[6] X.H. Min, S. Emura, T. Nishimura, K. Tsuchiya, K. Tsuzaki, Microstructure, tensile deformation mode and crevice corrosion resistance in Ti-10Mo-xFe alloys, Mater. Sci. Eng. 527 (2010) 5499–5506, https://doi.org/10.1016/j.msea.2010.06.016.
[7] X.H. Min, S. Emura, N. Sekido, T. Nishimura, K. Tsuchiya, K. Tsuzaki, Effects of Fe addition on tensile deformation mode and crevice corrosion resistance in Ti-15Mo alloy, Mater. Sci. Eng. 527 (2010) 2693–2701, https://doi.org/10.1016/j.msea.2009.12.050.
[8] H. Zhan, W. Zeng, G. Wang, D. Kent, M. Dargusch, On the deformation mechanisms and strain rate sensitivity of a metastable β Ti-Nb alloy, Scripta Mater. 107 (2015) 34–37, https://doi.org/10.1016/j.scriptamat.2015.05.014.
[9] H. Zhan, D. Kent, G. Wang, M.S. Dargusch, The dynamic response of a β titanium alloy to high strain rates and elevated temperatures, Mater. Sci. Eng. 607 (2014) 417–426, https://doi.org/10.1016/j.msea.2014.04.028.
[10] M. Hokka, T. Leemet, A. Shrot, M. Baeker, V.T. Kuokkala, Characterization and numerical modeling of high strain rate mechanical behavior of Ti-15-3 alloy for machining simulations, Mater. Sci. Eng. 550 (2012) 350–357, https://doi.org/10.1016/j.msea.2012.04.086.
[11] W.S. Lee, C.F. Lin, T.H. Chen, H.H. Hwang, Effects of strain rate and temperature on mechanical behaviour of Ti-15Mo-5Zr-3Al alloy, J. Mech. Behav. Biomed. Mater. 1 (2008) 336–344, https://doi.org/10.1016/j.jmbbm.2008.01.002.
[12] A. Paradkar, S.V. Kamat, The effect of strain rate on trigger stress for stress-induced martensitic transformation and yield strength in Ti-18Al-8Nb alloy, J. Alloys Compd. 496 (2010) 178–182, https://doi.org/10.1016/j.jallcom.2010.02.106.
[13] C. Li, J.H. Chen, X. Wu, S. van der Zwaag, Effect of strain rate on stress-induced martensitic formation and the compressive properties of Ti-V-(Cr,Fe)-Al alloys, Mater. Sci. Eng. 573 (2013) 111–118, https://doi.org/10.1016/j.msea.2013.03.002.
[14] S. Sadeghpour, S.M. Abbasi, M. Morakabati, Deformation-induced martensitic transformation in a new metastable β titanium alloy, J. Alloys Compd. 650 (2015) 22–29, https://doi.org/10.1016/j.jallcom.2015.07.263.
[15] X. Ji, S. Emura, X. Min, K. Tsuchiya, Strain-rate effect on work-hardening behavior in β-type Ti-10Mo-1Fe alloy with TWIP effect, Mater. Sci. Eng. 707 (2017) 701–707, https://doi.org/10.1016/j.msea.2017.09.055.
[16] M. Ahmed, D. Wexler, G. Casillas, D.G. Savvakin, E.V. Pereloma, Strain rate dependence of deformation-induced transformation and twinning in a metastable titanium alloy, Acta Mater. 104 (2016) 190–200, https://doi.org/10.1016/j.actamat.2015.11.026.
[17] R. Kapoor, A. Sarkar, J. Singh, I. Samajdar, D. Raabe, Effect of strain rate on twinning in a Zr alloy, Scripta Mater. 74 (2014) 72–75, https://doi.org/10.1016/j.scriptamat.2013.10.025.
[18] S. Sadeghpour, S.M. Abbasi, M. Morakabati, A. Kisko, L.P. Karjalainen, D.A. Porter, A new multi-element beta titanium alloy with a high yield strength exhibiting transformation and twinning induced plasticity effects, Scripta Mater. 145 (2018) 104–108, https://doi.org/10.1016/j.scriptamat.2017.10.017.
[19] P.J. Bania, Beta titanium alloys and their role in the titanium industry, J. Occup. Med. 46 (1994) 16–19, https://doi.org/10.1007/BF03220742.
[20] M. Morinaga, N. Yukawa, T. Maya, K. Sone, H. Adachi, Theoretical design of titanium alloys, in: Sixth World Conf. Titan. III, 1988, pp. 1601–1606. Cannes.
[21] M. Abdel-Hady, K. Hinoshita, M. Morinaga, General approach to phase stability and elastic properties of β-type Ti-alloys using electronic parameters, Scripta Mater. 55 (2006) 477–480, https://doi.org/10.1016/j.scriptamat.2006.04.022.
[22] J.H. Hollomon, Tensile deformation, Trans. Metall. Soc. AIME. 162 (1945) 268–290.
[23] F. Sun, J.Y. Zhang, M. Marteleur, T. Gloriant, P. Vermaut, D. Laillé, P. Castany, C. Curfs, P.J. Jacques, F. Prima, Investigation of early stage deformation mechanisms in a metastable β titanium alloy showing combined twinning-induced plasticity and transformation-induced plasticity effects, Acta Mater. 61 (2013) 6406–6417, https://doi.org/10.1016/j.actamat.2013.07.019.

[24] E. Bertrand, P. Castany, I. Péron, T. Gloriant, Twinning system selection in a metastable β-titanium alloy by Schmid factor analysis, Scripta Mater. 64 (2011) 1110–1113, https://doi.org/10.1016/j.scriptamat.2011.02.033.
[25] E. t Clementi, D.-L. Raimondi, Atomic screening constants from SCF functions, J. Chem. Phys. 38 (1963) 2686–2689.
[26] G. Testa, N. Bonora, A. Ruggiero, G. Iannitti, Flow stress of bcc metals over a wide range of temperature and strain rates, Met 10 (2020), https://doi.org/10.3390/met10010120.
[27] W. Zhou, K.G. Chew, The rate dependent response of a titanium alloy subjected to quasi-static loading in ambient environment, J. Mater. Sci. 37 (2002) 5159–5165.
[28] A. Ojha, H. Sehitoglu, Critical stresses for twinning, slip, and transformation in Ti-based shape memory alloys, Shape Mem. Superelasticity. 2 (2016) 180–195, https://doi.org/10.1007/s40830-016-0061-4.
[29] D.W. Brown, I.J. Beyerlein, T.A. Sisneros, B. Clausen, C.N. Tomé, Role of twinning and slip during compressive deformation of beryllium as a function of strain rate, Int. J. Plast. 29 (2012) 120–135, https://doi.org/10.1016/j.ijplas.2011.08.006.
[30] E.I. Galindo-Nava, P.E.J. Rivera-Díaz-Del-Castillo, Thermostastitical modelling of deformation twinning in HCP metals, Int. J. Plast. 55 (2014) 25–42, https://doi.org/10.1016/j.ijplas.2013.09.006.
[31] T. Wang, B. Li, M. Li, Y. Li, Z. Wang, Z. Nie, Effects of strain rates on deformation twinning behavior in α-titanium, Mater. Char. 106 (2015) 218–225, https://doi.org/10.1016/j.matchar.2015.05.016.
[32] R.W. Hertzberg, R.P. Vinci, J.L. Hertzberg, Deformation and Fracture Mechanics of Engineering Materials, fifth ed., Wiley, 2012. https://books.google.fi/books?id=8d8bAAAAQBAJ.
[33] R. Rajendran, M. Venkateshwarlu, V. Petley, S. Verma, Strain hardening exponents and strength coefficients for aeroengine isotropic metallic materials – a reverse engineering approach, J. Mech. Behav. Mater. 23 (2014) 101–106, https://doi.org/10.1515/jmbm-2014-0012.
[34] W.Q. Song, S. Sun, S. Zhu, G. Wang, J. Wang, M.S. Dargusch, Compressive deformation behavior of a near-beta titanium alloy, Mater. Des. 34 (2012) 739–745, https://doi.org/10.1016/j.matdes.2011.06.049.
[35] J. Talonen, P. Nenonen, G. Pape, H. Hänninen, Effect of strain rate on the strain-induced γ, → α′-martensite transformation and mechanical properties of austenitic stainless steels, Metall. Mater. Trans. A Phys. Metall. Mater. Sci. 36 A (2005) 421–432, https://doi.org/10.1007/s11661-005-0313-y.
[36] F. Peng, X.H. Dong, K. Liu, H.Y. Xie, Effects of strain rate and plastic work on martensitic transformation kinetics of austenitic stainless steel 304, J. Iron Steel Res. Int. 22 (2015) 931–936, https://doi.org/10.1016/S1006-706X(15)30092-3.
[37] R.K. Gupta, V.A. Kumar, C. Mathew, G.S. Rao, Strain hardening of titanium alloy Ti6Al4V sheets with prior heat treatment and cold working, Mater. Sci. Eng. 662 (2016) 537–550, https://doi.org/10.1016/j.msea.2016.03.094.
[38] L.C. Tsao, H.Y. Wu, J.C. Leong, C.J. Fang, Flow stress behavior of commercial pure titanium sheet during warm tensile deformation, Mater. Des. 34 (2012) 179–184, https://doi.org/10.1016/j.matdes.2011.07.060.
[39] Q. Wei, S. Cheng, K.T. Ramesh, E. Ma, Effect of nanocrystalline and ultrafine grain sizes on the strain rate sensitivity and activation volume: fcc versus bcc metals, Mater. Sci. Eng. 381 (2004) 71–79, https://doi.org/10.1016/j.msea.2004.03.064.
[40] R.S. Rosen, S.P. Paddon, M.E. Kassner, The variation of the yield stress of Ti alloys with strain rate at high temperatures, J. Mater. Eng. Perform. 8 (1999) 361–367, https://doi.org/10.1361/105994999770346927.
[41] C. Wang, N. Li, Y. Cui, M.T. Pérez-Prado, Effect of solutes on the rate sensitivity in Ti-xAl-yMo-zV and Ti-xAl-yMo-zCr β-Ti alloys, Scripta Mater. 149 (2018) 129–133, https://doi.org/10.1016/j.scriptamat.2018.02.028.
[42] D. Caillard, A TEM in situ study of alloying effects in iron. II—solid solution hardening caused by high concentrations of Si and Cr, Acta Mater. 61 (2013) 2808–2827, https://doi.org/10.1016/j.actamat.2013.01.049.
[43] K. Kapoor, P. Ravi, D. Naragani, J.-S. Park, J.D. Almer, M.D. Sangid, Strain rate sensitivity, microstructure variations, and stress-assisted β → α′′ phase transformation investigation on the mechanical behavior of dual-phase titanium alloys, Mater. Char. 166 (2020) 110410, https://doi.org/10.1016/j.matchar.2020.110410.
[44] Y. Yang, S.Q. Wu, G.P. Li, Y.L. Li, Y.F. Lu, K. Yang, P. Ge, Evolution of deformation mechanisms of Ti-22.4Nb-0.73Ta-2Zr-1.34O alloy during straining, Acta Mater. 58 (2010) 2778–2787, https://doi.org/10.1016/j.actamat.2010.01.015.
[45] Y. Yang, P. Castany, M. Cornen, F. Prima, S.J. Li, Y.L. Hao, T. Gloriant, Characterization of the martensitic transformation in the superelastic Ti-24Nb-4Zr-8Sn alloy by in situ synchrotron X-ray diffraction and dynamic mechanical analysis, Acta Mater. 88 (2015) 25–33, https://doi.org/10.1016/j.actamat.2015.01.039.
[46] P. Castany, A. Ramarolahy, F. Prima, P. Laheurte, C. Curfs, T. Gloriant, In situ synchrotron X-ray diffraction study of the martensitic transformation in superelastic Ti-24Nb-0.5N and Ti-24Nb-0.5O alloys, Acta Mater. 88 (2015) 102–111, https://doi.org/10.1016/j.actamat.2015.01.014.
[47] J. Gao, Y. Huang, D. Guan, A.J. Knowles, L. Ma, D. Dye, W.M. Rainforth, Deformation mechanisms in a metastable beta titanium twinning induced plasticity alloy with high yield strength and high strain hardening rate, Acta Mater. 152 (2018) 301–314, https://doi.org/10.1016/j.actamat.2018.04.035.
[48] F. Sun, J.Y. Zhang, M. Marteleur, C. Brozek, E.F. Rauch, M. Veron, P. Vermaut, P. J. Jacques, F. Prima, A new titanium alloy with a combination of high strength, high strain hardening and improved ductility, Scripta Mater. 94 (2015) 17–20, https://doi.org/10.1016/j.scriptamat.2014.09.005.
[49] X. Min, X. Chen, S. Emura, K. Tsuchiya, Mechanism of twinning-induced plasticity in β-type Ti-15Mo alloy, Scripta Mater. 69 (2013) 393–396, https://doi.org/10.1016/j.scriptamat.2013.05.027.
[50] S. Hanada, A. Takemura, O. Izumi, The mode of plastic deformation of beta Ti-V alloys, Trans. Japan Inst. Met. 23 (1982) 507–517, https://doi.org/10.2320/matertrans1960.23.507.
[51] J.D. Cotton, R.D. Briggs, R.R. Boyer, S. Tamirisakandala, P. Russo, N. Shchetnikov, J.C. Fanning, State of the art in beta titanium alloys for airframe applications, JOM (J. Occup. Med.) 67 (2015) 1281–1303, https://doi.org/10.1007/s11837-015-1442-4.